Noise-enhanced neuronal reliability

Seiji Tanabe
Department of Systems and Human Science, School of Engineering Science, Osaka University, Toyonaka 560-8531 Osaka, Japan

K. Pakdaman
Inserm U444, Faculté de Médecine Saint-Antoine, 27, rue Chaligny, 75571 Paris Cedex 12, France

(Received 23 April 2001; revised manuscript received 25 June 2001; published 20 September 2001)

This work shows that noise can enhance the discharge time reliability in Hodgkin-Huxley neuron models stimulated by weak periodic and aperiodic inputs. By expanding the Fokker-Planck equation of an elementary model for excitable systems, the dependence of the optimal noise intensity on input characteristics is discussed.

DOI: 10.1103/PhysRevE.64.041904 PACS number(s): 87.17.Aa, 05.40.−a, 87.10.+e

I. INTRODUCTION

Signal processing in nervous systems takes place in the presence of external perturbations and internal fluctuations, broadly referred to as noise [1]. Neurons are nonlinear devices whose response can be strongly affected by the noise [2]. Surprisingly, such alterations are not necessarily detrimental. Numerous studies [3,4], supported by behavioral evidence [5], have established that noise can play a positive functional role by assisting neurons in the detection or transmission of weak inputs. Such observations have opened the door to possible biomedical applications [6]. One of the mechanisms accounting for the role of noise is through the reduction of nonlinear distortions between stimuli and the discharge rate of neurons [2,7–9], which improves input-output fidelity. In this sense, noise can assist ''rate coding.''

In many instances, rapid and precise computations in nervous systems rely on a different code, namely temporal coding [10]. In this case, the stimulus characteristics are encoded into discharge timings rather than averaged firing rates. To operate such a code, a neuron must be reliable in the sense that there must be little variability in the discharge times evoked by repetitive presentation of a given input ([11–13] and the review [14]). Otherwise, distinction between different signals is not possible from the observation of the discharge times. Given that jitter in the spike timing deteriorates temporal code, the prevailing view is that noise is one of the key limiting factors in the operation of such codes [15,16].

The main purpose of the present paper is to show that this is not necessarily so. More precisely, in the same way that noise can enhance neuronal fidelity, it can also enhance its discharge time reliability to weak inputs. To this end, we first examine the influence of noise on the discharge times of a weakly forced canonical neuron model, namely the Hodgkin-Huxley (HH) model [17]. Previous studies have reported that noise can increase spike timing precision in ensembles of HH units stimulated by a single-weak excitatory post synaptic potential [18–20]. Analyzing the response to this form of input is a first step towards characterizing the influence of noise on temporal coding. In contrast with these, the present study deals with periodic and aperiodic input signals similar to the ones that occur in nervous systems. More precisely, periodic modulations have been observed in systems such as the owl auditory system [21] and the electrosensory system of electric fish [22], both of which perform highly precise computational tasks, and aperiodic ones are common in cortical neurons as a result of the large number of connections such neurons receive [23].

Finally, we support our numerical investigations in the HH model by analyzing noise enhanced reliability using the Fokker-Planck equation (FPE) of the active rotator (AR) [20,24–27], an elementary model for excitable systems widely used in the determination of the influence of noise. Furthermore, this enables us to discuss the dependence of the optimal noise level on input period and amplitude. This is an issue of importance (i) to determine whether nervous systems operate in conditions suitable for noise-enhanced reliability, and (ii) for potential usage of noise in biomedical devices if improved reliability is desirable.

This paper is organized as follows. First the influence of noise on reliability in the HH model is presented and compared with enhanced fidelity (Sec. II). Then, the same phenomenon is analyzed in the AR, using the FPE and its expansions (Sec. III). Finally conclusions are presented (Sec. IV).

II. THE HODGKIN-HUXLEY MODEL

We report simulation results of the HH model (Appendix A) under two conditions: one receiving sinusoidal input and another receiving aperiodic input. The aperiodic signal was a sample path of an Ornstein-Uhlenbeck process.

Two quantities were computed to evaluate the relation between the input signals and the spike train generated by the HH model. One is the input-output correlation C_0, and the other the discharge time reliability R_{el}.

The first one measures input-output fidelity defined as the linear correlation between the input $s(t)$ and the output $y(t)$ [7,9]

$$C_0 = \max_{\tau} \{\overline{s(t)y(t+\tau)}\}, \tag{1}$$

where the overbar denotes average over several independent trials. For a periodic input $s(t)=A\sin(\Omega t)$, we evaluate C_0 as [9]

$$C_0 = \max_{\tau}\left\{\frac{1}{T}\int_0^T A\sin(\Omega u)y(u+\tau)du\right\}$$
$$= A\sqrt{\alpha_1^2+\beta_1^2}/2, \quad (2)$$

where $T=2\pi/\Omega$ is the stimulation period, and α_1 and β_1 are the first Fourier coefficients of the output $y(t)$ computed as

$$\alpha_1 = \overline{\frac{2}{T}\int_0^T \cos(\Omega t)y(t)dt}, \quad (3)$$

$$\beta_1 = \overline{\frac{2}{T}\int_0^T \sin(\Omega t)y(t)dt}. \quad (4)$$

Conversely, for an aperiodic input $s(t)$, we computed C_0 as

$$C_0 = \overline{\frac{1}{T}\sum_{m=1}^{M} s(t_m)}, \quad (5)$$

where t_m ($m \in [1,2,\ldots,M]$) are the time of discharges and T is the duration of the aperiodic stimulus. This is the cross correlation between output spike train and the input signal evaluated at zero time delay. It measures whether the number of spikes fired within some time interval reflects the variation in the input signal. Roughly speaking, a large positive C_0 indicates that the increases and decreases in the input are concurrent with similar evolutions in the firing rate.

The standard experimental protocol to evaluate neuronal reliability consists in presenting repetitively a given stimulation segment to a neuron. Then the discharge times in each trial, measured from the stimulation onset, are compared with one another. When the discharges of the different trials are aligned, the discharge timing is referred to as precise and the firing as reliable. The above procedure has been widely used in experiments dealing with various levels of signal processing in nervous systems [11–13]. Besides a qualitative assessment of reliability, various quantities have been used to quantify this property [12,13,18].

The first step in the evaluation of these quantities is to ''pool'' the spike trains from the independent trials together, in other words, to consider the point process formed by summing the point processes representing the discharge times during each trial. From a modeling point of view, this is equivalent to considering the pooled spike train generated by an ensemble of noninteracting units, receiving all the same input signal, so that our work applies both to the reliability of single units and to synchronous firing within ensembles.

The second step for measuring reliability consists in estimating the instantaneous firing rate of the pooled spike train or, equivalently, of the ensemble. This is done by convolving the point process with a filter. Various filters have been used in previous studies [12,13,18]. One purpose for filtering the spike train is to smooth the data. However, the key argument for selecting a filter is that discharge times from trial to trial or coming from different neurons within an ensemble are unlikely to be perfectly aligned, but they can occur close enough to one another so that their influences on a downstream neuron effectively add up. Filtering the spike train allows the addition of the effects of nearby discharges in the same way as in postsynaptic membranes. Based upon this consideration, we follow Hunter *et al.* [13] in that, when needed, we filter spike trains with an exponential filter. This choice is motivated by two factors, one that the exponential filter is a reasonable approximation of the postsynaptic effect of a presynaptic firing, and, the other, that it is computationally advantageous for rapid estimation of the instantaneous firing rate.

The third step for evaluating reliability consists in computing the measure itself. While several different measures have been used [9,12,13,18], they are all based upon one key consideration, which is also the fundamental difference between these measures and others such as correlation C_0. More precisely, the reliability measures quantify the sharpness and sizes of peaks of the instantaneous firing rate, *regardless* of the input signal. In other words, these measures indicate whether discharges in the pooled spike train were synchronous (after the filtering). They do not measure whether these synchronous firings occur when the input signal presents, say, a transient increase, or any other specific feature. In this sense, high reliability measures indicate that to a given stimulation there corresponds a given sequence of discharge times, so that temporal coding is possible for such classes of inputs. However, these measures do not shed light on the ''coding'' relation between the input signal and the spike train. This contrasts with a measure such as C_0, which evaluates whether there is a linear relation between the input signal and the firing rate.

In the following, we detail the reliability measure used in our paper, which is the one introduced by Hunter *et al.* [13]. The reliability R_{el} measures the propensity of neurons within an ensemble to fire synchronously in response to a given stimulation, or equivalently, that of a given neuron to fire at the same times when stimulated by the same input. The computation of the reliability is based upon that of the variance ρ^2 of the output $y(t)$.

The output $y(t)$ is convolved with an exponential filter as

$$y_f(t) = \int_0^t y(t-\tau)\lambda\exp[-\lambda\tau]d\tau = \lambda\sum_{m=1}^{M}\exp[-\lambda(t-t_m)],$$

where $1/\lambda$ is the characteristic time of the synchrony among the ensemble. Substituting $y(t)$ with $y_f(t)$, we have

$$\rho^2 = \overline{\frac{1}{T}\int_0^T y_f^2(t)dt - \left[\frac{1}{T}\int_0^T y_f(t)dt\right]^2}. \quad (6)$$

Using the above, the reliability is defined as

$$R_{el} = \rho^2/\overline{N}, \quad (7)$$

where, for a periodic input, $\overline{N}$ is the mean number of discharges per input period, while for an aperiodic input, it represents a normalization factor, computed as: $N^2M\lambda/(2T) - N^2M^2/T^2$ where T is the simulation duration, M is the number of spikes, and N the number of spike trains [13]. For a periodic input, R_{el} can be expressed in terms of the Fourier coefficients α_k and β_k of the unfiltered signal y as

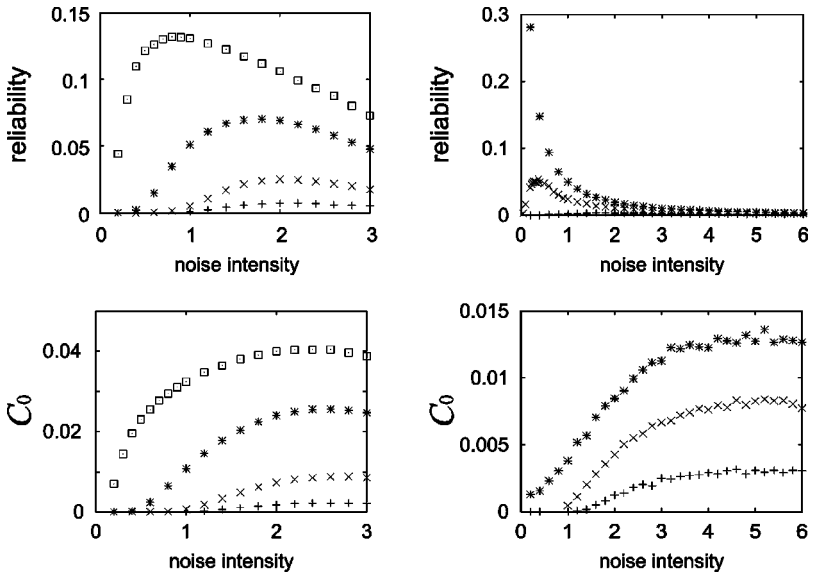

FIG. 1. Reliability and C_0 to periodic and aperiodic input in an HH model. Reliability (top row) and C_0 (bottom row) as a function of noise intensity. Input currents are a sinusoid (left column) and sample path of an Ornstein-Uhlenbeck process (right column). All abscissas are $(\mathrm{mA}\sqrt{\mathrm{ms}}/\mathrm{cm}^2)$. Ordinates in the upper row are unitless, and in the lower row are $\mathrm{mA}/(\mathrm{ms}\times\mathrm{cm}^2)$. Stimulus parameters for periodic input are $\Omega=0.22$ (rad/ms), $A=0.4$ (+),0.8 (×), 1.4 (∗), and 1.8 (□) $(\mathrm{mA}/\mathrm{cm}^2)$, and those for aperiodic input are time constant $\tau=1$ (ms), and $A=0.8$ (+),1.5 (×), and 2 (∗) $(\mathrm{mA}/\mathrm{cm}^2)$. The time-scale parameter λ of reliability are 5 and 1 (ms^{-1}) for periodic and aperiodic inputs, respectively. Simulations of 2000 (left column) and 1000 (right column) HH units were run and the output spike train of all units were pooled to form a single spike train. All simulations were started at the resting state and run using the standard Euler method with a time step of 0.005 ms for a duration of 50 input cycles (left column) and 1 s (right column), respectively. Transient spikes were not discarded. Discharges were defined as the membrane potential crossing upwards through 50 mV at least 3 ms after the previous discharge.

$$R_{el}=\frac{2}{\alpha_0(\lambda-\alpha_0)}\sum_{k\geqslant 1}\frac{\lambda^2}{\lambda^2+k^2\Omega^2}(\alpha_k^2+\beta_k^2). \tag{8}$$

For subthreshold periodic or aperiodic inputs, both C_0 and R_{el} have a nonmonotonic dependence on the noise intensity. They both decay at low and large noise intensities, and present a unique maximum at an intermediate noise level (Fig. 1). For C_0, this is noise-enhanced fidelity, a phenomenon that has been previously studied in detail [7–9]. The lower maximal C_0 associated with the aperiodic input is mainly due to the fact that this signal contains much faster frequency components than the periodic one, and that these high frequencies are poorly transmitted by neurons. Thus, the fidelity is lower in the aperiodic case compared with the periodic.

That R_{el} is maximal at an intermediate noise level, i.e., noise-enhanced reliability, constitutes a different effect of noise on neuronal coding. Comparison between noise-enhanced fidelity and reliability highlights the key similarities and differences between these two phenomena.

Besides the fact that, for weak inputs, when plotted as a function of noise intensity, C_0 and R_{el}, both exhibit a hump-like shape, these two quantities display similar dependence on input intensity. When the latter is increased, C_0 and R_{el}, both increase at all noise levels. However, the optimal noise intensities at which maximal fidelity and reliability are reached differ. The former is substantially larger than the latter, and the difference widens with the input amplitude. Maximal fidelity is reached for roughly the same noise level at all input amplitudes. This is not the case for maximal reliability: the optimal noise level tends to zero as the signal reaches threshold level. This tendency is common in both periodic and aperiodic input conditions.

III. THE ACTIVE ROTATOR

Our numerical analysis of the response of the HH model established that noise enhanced-reliability occurs for both periodic and aperiodic signals, and revealed the similarity between these two cases. Our main concern in the remainder of this paper is to investigate the mechanisms underlying noise-enhanced reliability. To this end, we focus on periodic stimulation applied to the noisy AR, a simplified model for excitable systems.

The state of an AR model is defined by a point φ on a unit circle. The autonomous dynamics are given by $d\varphi/dt=1-a\sin(\varphi)$, so that when $a>1$, there are two fixed points, one stable and the other unstable. A state starting at all points along the circle except the unstable point eventually asymptotes to the stable point. The unstable point acts as a threshold of an excitable system because points starting at opposite sides of the unstable point return to the resting state in opposite rotation. The dynamics of an AR receiving a periodic input and noise is then governed by

$$\frac{d\varphi}{dt}=1-a\sin(\varphi)+A\sin(\Omega t)+\xi(t), \tag{9}$$

where ξ is white Gaussian noise, satisfying $E[\xi(t)]=0$ and $E[\xi(t)\xi(s)]=2D\delta(t-s)$. The Fokker-Planck equation associated with Eq. (9) is [20,24–27]:

$$\frac{\partial n}{\partial t}(\varphi,t) = -\frac{\partial F}{\partial \varphi}(n(\varphi,t),t) \tag{10}$$

$$= L_0[n(\varphi,t)] + AL_{ext}[n(\varphi,t),t], \tag{11}$$

where $n(\varphi,t)d\varphi$ represents the proportion of units within $(\varphi,\varphi+d\varphi)$ at time t and $F[n(\varphi,t),t]=[1-a\sin(\varphi)+A\sin(\Omega t)]n(\varphi,t)-D(\partial n/\partial\varphi)(\varphi,t)$ is the flux. In Eq. (11), L_0 and L_{ext} represent the autonomous and input-dependent components of the right-hand side of the FPE

$$L_0(n) = \frac{\partial}{\partial \varphi}\left\{ -f(\varphi)\, n + D\frac{\partial}{\partial \varphi} n \right\}, \tag{12}$$

$$L_{ext}(n,t) = -\sin(\Omega t)\frac{\partial n}{\partial \varphi}, \tag{13}$$

where $f(\varphi)=1-a\sin(\varphi)$.

The output rate $J(t)$ of the AR can be computed from the solution of the FPE as the flux through $3\pi/2$, that is, $J(t)=F[n(3\pi/2,t),t]$. From this, we compute the input-output correlation C_0 and the reliability R_{el} using Eqs. (2) and (8) with α_k and β_k representing the kth Fourier coefficients of J.

We systematically computed the flux of an AR model receiving periodic modulation for various noise intensities and modulation amplitudes [28]. Control cases were also computed from numerical simulations of periodically forced noisy AR's, and satisfactory correspondence between these quantities and the estimates from the flux of the FPE was observed (not shown). Figure 2 shows that this system reproduces the behavior of the HH model in the sense that (i) both C_0 and R_{el} are hump-shaped when plotted against noise intensity and (ii) the curves display similar dependence on input amplitude as for the HH. The amplitude of the stimulation for the AR model was close to sixfold smaller than that for the HH model. Therefore, while the ranges of C_0 in the two models are different, those of $\sqrt{\alpha_1^2+\beta_1^2}$ are of the same order.

Using the FPE of the AR, we examined the dependence of the optimal noise levels maximizing C_0 and R_{el} on input amplitude. Figure 3 summarizes the results of the numerical investigations. The loci of the optimal noise maximizing reliability R_{el} and C_0 (represented, respectively, by ● and ○ in Fig. 3) are plotted in the *D*-*A* plane, where *D* is the noise intensity and *A* is the input amplitude. Similar to HH model simulations, the reliability had a peak at smaller noise compared to C_0. The dependence of these peaks on the input amplitude was also reproduced in the AR model. The optimal noise intensity of reliability shifted towards zero noise as modulation amplitude was increased, in contrast with that of C_0, which remained within an intermediate range, even when modulation reached suprathreshold levels. This difference is in fact a reflection of the differences in the mechanisms underlying noise-enhanced reliability and the well-documented linearization by noise. In the following, we investigate the noise-induced changes in neuronal behavior that are responsible for enhanced reliability.

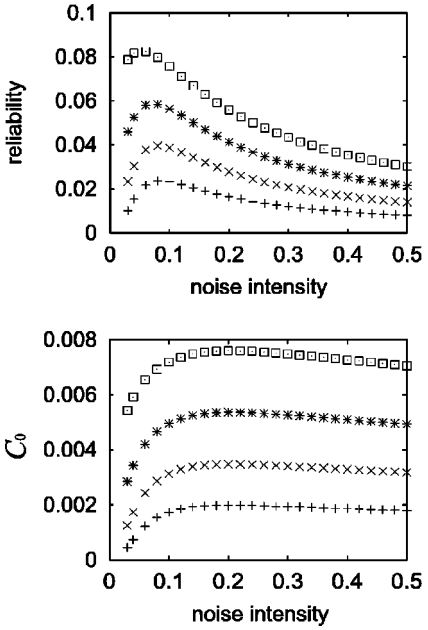

FIG. 2. Reliability and C_0 to periodic input in an AR model. Reliability (upper panel) and C_0 (lower panel) as a function of noise intensity. Input currents are a sinusoid of angular velocity $\Omega=0.3$ [rad/ms] and amplitudes $A=0.15$ (+), 0.20 (×), 0.25 (∗), and 0.30 (□) (rad/ms), respectively. Abscissas in both panels are noise intensity (rad/$\sqrt{\text{ms}}$) and ordinates are dimensionless (upper panel) and rad/ms^2. Both reliability and C_0 were computed from the flux crossing $\varphi=3\pi/2$. The time-scale parameter λ of reliability is (ms^{-1}). Numerical computations of the flux were carried out by simulating the approximation of the FPE using the fourth-order Runge-Kutta method with a time step of 0.01 ($D\leqslant 0.3$) and 0.005 ($D>0.3$). All Fourier coefficients of the probability density function, expanded up to 30th order, were initialized at zero. After running 50 ms, data points over a duration of 5 input cycles were analyzed. The single AR model parameter is $a=1.2$.

Our starting point is our previous studies [19,20,29] that revealed that (i) canonical neuronal models such as the HH equations, the AR but also the FitzHugh-Nagumo model, and the leaky integrate and fire unit, all undergo a noise-induced transition as noise intensity is increased, and (ii) this phe-

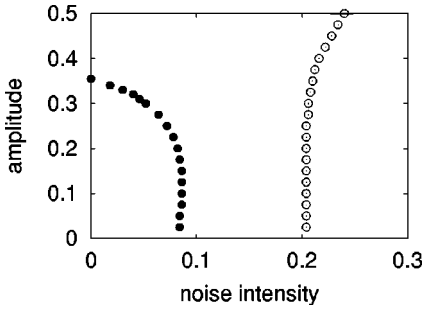

FIG. 3. Optimal noise at various input amplitudes in an AR model. Each point is plotted at the noise intensity where reliability (●) and C_0 (○) are maximal for each input amplitude. The abscissa is noise intensity (rad/$\sqrt{\text{ms}}$) and the ordinate is modulation amplitude (rad/ms). The model and simulation parameters are the same as in Fig. 2.

nomenon accounts for the noise enhanced discharge time precision in response to a single subthreshold postsynaptic potential. In the following, we show that a similar mechanism accounts for enhanced reliability in response to other classes of stimuli such as subthreshold periodic ones. To this end, we proceed as follows. The noise induced-transition is characterized by a change in the stationary distribution of model variables from Gaussian-like to non-Gaussians. We have shown that a signature of this transition is a bifurcation in the deterministic equations approximating the dynamics of the moments (the means and variances) of the model variables prior to the transition. Since our previous studies [19,20,29] considered the effect of noise alone on these systems, it is not possible to directly apply the results to units receiving, say, a maintained periodic current stimulation. To address this issue, we need to consider the moment equations in the presence of both the noise and the external input. This is done in the case of the periodically forced AR in the following.

The key observation that allows the derivation of the moment equations is that at low-noise intensities, the density $n(\varphi,t)$ solution of Eq. (11) is well approximated by a Gaussian. In other words, given a single realization of the forced AR receiving a weak noise, the probability that at time t, the AR is within some phase range $(\varphi,\varphi+d\varphi)$ is given by $n(\varphi,t)d\varphi$ where, under the Gaussian assumption

$$n(\varphi,t)\simeq\frac{1}{\sqrt{2\pi v(t)}}\exp\left\{-\frac{1}{2}\frac{[\varphi-u(t)]^2}{v(t)}\right\}, \qquad (14)$$

where $u(t)$ and $v(t)$ represent the mean and variance of $\varphi(t)$. Equivalently, given a large ensemble of noninteracting AR's, the proportion of units whose phase is within $(\varphi,\varphi+d\varphi)$ is given by $n(\varphi,t)d\varphi$. For the unforced AR, this assumption has been used in our previous study [20]. This approximation also applies to the forced AR, as a special case from a general result on weak white-noise perturbations of dynamical systems [30].

The dynamics of the mean and variance of n are given by:

$$\frac{du}{dt}=1-aE[\sin(\varphi)]+A\sin(\Omega t), \qquad (15)$$

$$\frac{dv}{dt}=-2aE[(\varphi-u)\sin(\varphi)]+2D, \qquad (16)$$

where E denotes expectation. Using Eq. (14), we can evaluate Eqs. (15)–(16) as [25,20]

$$\frac{du}{dt}=1-a\sin(u)\exp\left(-\frac{v}{2}\right)+A\sin(\Omega t), \qquad (17)$$

$$\frac{dv}{dt}=-2a\cos(u)v\exp\left(-\frac{v}{2}\right)+2D. \qquad (18)$$

When $A=0$, solutions of Eqs. (17) and (18) display one of two behaviors depending on the value of D. More precisely, they remain bounded or diverge for noise intensities below and beyond the noise induced transition, respectively. The separation between these two different asymptotic behaviors comes in the form of a deterministic bifurcation [20,29]. We have observed a similar separation in the presence of periodic forcing, i.e., $A\neq 0$. The following paragraphs describe this aspect and discuss its relation with enhanced reliability.

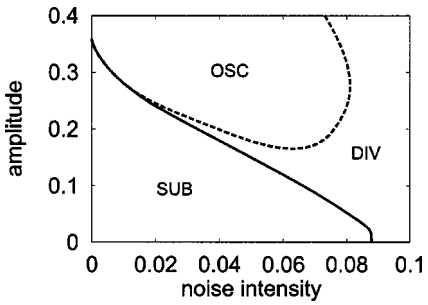

FIG. 4. Various dynamics of the moments of an AR model. Regions where the mean $u(t)$ remains subthreshold (SUB), where $u(t)$ oscillates around the circle while variance $v(t)$ remains bounded (OSC), and where both $u(t)$ and $v(t)$ diverge to nonnumerical values (DIV) are delineated in the input amplitude A versus noise intensity D two-parameter plane. The abscissa is noise intensity (rad/$\sqrt{\text{ms}}$) and the ordinate is modulation amplitude (rad/ms). The time step is 0.01 ms. Model and input parameters are the same as in Fig. 2.

When $A\neq 0$, solutions of Eqs. (17)–(18) display one of three behaviors depending on the values of D and A. These are (i) for low A and D (lower-left region in Fig. 4), bounded oscillations of both u and v, with u oscillating around the stable fixed point of the unforced AR, (ii) for large A, and small D (upper-left region in Fig. 4), u rotates around the unit circle, while v displays bounded oscillations, and (iii) for large D (right region in Fig. 4), the two variables u and v diverge. In the first regime, firing is sparse and the AR displays mainly subthreshold oscillations. In the second region, firing takes place, either because A is suprathreshold or because there is enough noise. However, the fact that v remains bounded reflects the fact that the noise is not large enough to completely dominate the firing. This latter situation takes place in the third region.

The noise-induced transition corresponds to the border delineating the first region. It represents the change in the system from a mainly subthreshold regime to one in which firing takes place. Remarkably, the locus of this border in the D-A plane is similar to the locus of the optimal noise levels obtained directly from the FPE (Fig. 3). The quantitative difference between the two curves is due to two factors. One comes from the fact that Eqs. (15)–(16) are an approximation that captures mainly qualitative changes in the system behavior rather than quantitative changes. The other is that, in fact, maximal reliability is reached after the onset of firing at the noise-induced transition, so that the optimal noise levels are larger than the ones corresponding to the noise-induced transition.

The reason why the noise-induced transition separates the regions in which the noise improves and deteriorates neuronal reliability can be understood from the characteristics of the two regimes. In the first one, the sensitivity of neurons to weak inputs increases due to the noise-induced fluctuations

that bring the system close to its firing threshold. The key point here is that in this regime, noise alone causes little firing, so that the discharges are mainly due to the input signal, and therefore, evoke reliable firing. Conversely, in the second regime, the firing is mainly due to the noise rather than the input signal. This phenomenon accounts for the decrease in reliability.

The above analysis clarified the mechanism underlying noise-enhanced reliability in the AR, and the dependence of the optimal noise on input amplitude. In the following, we address a different question, that of the dependence of the optimal noise on the input period. In this case, we focus on weak inputs. Figure 3 shows that, for such inputs, the optimal noise depends little on the modulation amplitude. We apply the linear response theory to analyze the conditions for getting high reliability or high C_0.

At the limit of small modulation amplitude A, we expand n and J as

$$n(\varphi,t)=n_0(\varphi)+An_1(\varphi,t)+A^2n_2(\varphi,t)+\cdots,$$

$$J(t)=J_0+AJ_1(t)+A^2J_2(t)+\cdots. \tag{19}$$

Substituting these into Eq. (11), and regrouping the terms with the same order in A, yields the following system governing the dynamics of the terms in the expansion:

$$\frac{\partial n_0}{\partial t}-L_0[n_0]=0,$$

$$\frac{\partial n_1}{\partial t}-L_0[n_1]=L_{ext}[n_0,t],$$

$$\vdots,$$

$$\frac{\partial n_k}{\partial t}-L_0[n_k]=L_{ext}[n_{k-1},t]. \tag{20}$$

We numerically simulated the above system and checked that for small amplitudes A, the solution up to the first order provided a satisfactory approximation of the solution of Eq. (11) [31]. Furthermore, by progressively increasing the value of A, we checked that, while the validity of the first-order approximation deteriorated, by increasing the order of the expansion, one could always obtain a satisfactory approximation. This could be seen, for instance, from the observation that, when plotted together, the graphs of $J(t)$ against time, computed directly from Eq. (11) and from the expansion, could not be visually distinguished from one another. Finally, we also checked that the approximate values of the measures C_0 and R_{el} obtained from the expansion matched those obtained with Eq. (11). These numerical comparisons showed that the expansion provides a satisfactory approximation of the original system. In the following, we describe only results obtained with the first-order term, which highlight the dependence of the optimal noise intensity on input period.

In the stationary regime, n_0 tends to n_0^*, the stationary probability density function of the unforced AR [27,20], and

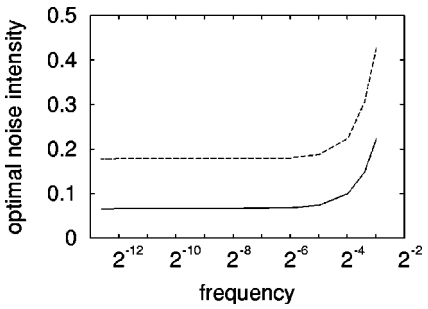

FIG. 5. Optimal noise as a function of input frequency in an AR model. The curve is plotted at the noise intensity where reliability (solid) and C_0 (dashed) are maximal as a function of input frequency. The abscissa is noise intensity (rad/$\sqrt{\text{ms}}$) and ordinate is modulation frequency (kHz). Both reliability and C_0 were computed from the flux crossing $\varphi=3\pi/2$ in the first-order perturbation with arbitrary input amplitude. Numerical computations were carried out by simulating the expansion of the FPE using the standard Euler method with a time step of 0.005. All Fourier coefficients of the probability density function, expanded up to 30th order, were initialized at the asymptotic solution of FPE in the absence of modulation. After running 50 ms, data points over a duration of 50 ms were analyzed. Model parameters are the same as in Fig. 2.

n_1 takes on the form $n_1(\varphi,t)=x(\varphi)\cos(\Omega t)+z(\varphi)\sin(\Omega t)$, where x and z satisfy the following system of linear ordinary differential equations:

$$D\frac{d^2x}{d\varphi^2}=\frac{d}{d\varphi}[(1-a\sin(\varphi))x]+\Omega z, \tag{21}$$

$$D\frac{d^2z}{d\varphi^2}=\frac{d}{d\varphi}[(1-a\sin(\varphi))z]-\Omega x+\frac{dn_0^*}{d\varphi}. \tag{22}$$

The stationary linear response does not contain any terms with higher harmonics. These higher harmonics appear progressively if one proceeds further with the expansion. The same goes for the expansion of the rate J. In the stationary regime, J_0 is constant and $J_1(t)=\alpha\cos(\Omega t)+\beta\sin(\Omega t)$. The coefficients α and β can be directly evaluated from x and z. In this way, from Eqs. (2) and (8), the expansions of C_0 and R_{el} are

$$C_0=\frac{A^2}{2}\sqrt{\alpha^2+\beta^2}, \tag{23}$$

$$R_{el}=\frac{2\lambda^2A^2}{\alpha_0(\lambda-\alpha_0)(\lambda^2+\Omega^2)}(\alpha^2+\beta^2), \tag{24}$$

where α_0 depends neither on A nor Ω, and only on D, and α and β do not depend on A, but only on Ω and D.

Using these expressions, we have numerically computed the optimal noise intensities that maximize C_0 and R_{el} for different input periods. The dependency of the optimal noise level to the input frequency is shown in Fig. 5 for both C_0 (solid curve) and R_{el} (dashed curve). The results show that up to about $\Omega=0.2$, the optimal noise level is almost the

same no matter how slow the input is. As the frequency is increased beyond this value, the optimal noise intensity also increases.

These results can be interpreted as follows. For low-input frequencies, the optimal noise does not depend on Ω, because the system behavior can be studied through a quasistationary assumption. For linearization by noise, this has been previously described in [8]. For enhanced reliability, this means that the input term in Eqs. (17)–(18) varies so slowly, that the noise-induced transition occurs at the same noise level as for a constant input, and therefore displays little dependence on input frequency.

One factor influencing the increase of the optimal noise at higher frequencies is the AR's cutting frequency: the amplitude of subthreshold oscillations decreases with input frequency, and this effect is more marked for frequencies higher than a critical value. This is due to the properties of the AR linearized at its stable equilibrium point. In this way, keeping A fixed, while increasing Ω results in smaller effective oscillations in φ, thus requiring larger noise intensities to induce firing, and henceforth, resulting in larger optimal noise levels for both C_0 and R_{el}.

The above result highlights that, for weak inputs, the dependence of the optimal noise intensity on input frequency reflects mainly the subthreshold response of the system near the equilibrium point. This effect is similar to what has been discussed in conventional stochastic resonancelike phenomena in the leaky integrate and fire model [32] and the FitzHugh-Nagumo model [4].

IV. DISCUSSION

While spike trains constitute one of the main information carriers in nervous systems, the encoding of input signals into such pulse sequences can take on different forms (e.g., [10,33,34]). Two of these are rate and temporal coding. In the former, the mean discharge rate of neurons conveys information about the input signal, while in the latter, it is the sequence of discharge times that fills in this role. This study investigated the influence of noise on two quantities, the linear correlation C_0 and the reliability R_{el}, which are measures related to these two forms of coding, rate coding and temporal coding. In agreement with previous studies [7–9], we observed that for weak inputs, some intermediate noise level maximizes C_0. We also reported that under the same conditions, some noise also enhances neuronal reliability. However, the noise intensities at which these occur widely differ from one another. The following paragraphs discuss the main aspects of enhanced fidelity and reliability and clarify the differences between the two.

The measure C_0 quantifies the linear relation between the input signal and the neuron's firing rate. For weak inputs, C_0 takes low values because the response of the neuron is rectified, that is, only the suprathreshold segments of the signal evoke discharges. The addition of some noise increases C_0 because it allows some firing to take place even for subthreshold signal segments, with a rate that is commensurate with the distance of the stimulus to the threshold. While further increase in the noise further attenuates the nonlinear distortions, it also introduces random fluctuations that deteriorate C_0. The humplike dependence of C_0 on noise intensity reflects the competition between these two effects [8,9]. Thus, the main phenomenon that accounts for enhanced fidelity is that noise reduces the nonlinear distortions in the input-output relation of neurons such as the ones caused by the threshold. For this reason, it is referred to as linearization by noise [2].

Conversely, in the case of enhanced reliability for weak inputs, the effect of noise strongly depends on the threshold. The key point here is that due to threshold, membrane potential fluctuations abruptly increase as the system enters the noise-induced transition regime. These large fluctuations reflect neuronal firing. So, in effect, for a given noise level, firing is possible only in segments of the signal that are beyond the transition. For low noise, there are no such segments when the input is subthreshold. When the noise is increased, only a few, clearly separated input segments are above the transition, so that action potentials can take place only in these intervals: the firing is reliable. However, as noise is further increased, so does the length of the ''supratransition'' segments, making it possible for several spikes to occur in each. The timing of these fluctuates because in the supratransition range, firing is mainly caused by noise. Thus, the abruptness of the noise-induced transition plays an important role in noise-enhanced reliability: it allows firing to occur in some specific preferential input segments, and therefore be reliable.

The above descriptions clarify the difference between the noise ranges where enhanced fidelity and reliability are reached. We observed that the noise level maximizing C_0 did not go to zero when the signal amplitude was increased until threshold. This is because even for suprathreshold stimulation, the neuronal firing rate can present strong nonlinear distortions due to rectification. Some amount of noise reduces these distortions and therefore improves fidelity. In contrast, the optimal noise maximizing the reliability tends to zero with the signal amplitude. This is because as the signal amplitude is increased, lower noise levels are required to have ''supratransition'' input segments that are wide enough to allow firing and not too wide to have several discharges. At such noise intensities, the firing is highly reliable firing with poor fidelity due to the rectification. This accounts for the difference between the two optimal noise intensities.

Finally, we examine the implication of the above analysis in terms of neuronal coding. High fidelity attained when C_0 is maximal means that there is a large linear correlation between the input signal and the output of the neuron. In such a case, one can assume that the main function of the neuron is to transmit the input signal with as little distortion as possible. As this is best achieved by a linear system, neuronal nonlinearities, such as the threshold, hinder transmission fidelity. In this setting, noise may play a significant functional role through linearization. Conversely, highly reliable firing is achieved in a regime where the input-output fidelity can be poor. In this case, firing reliability indicates that the input is encoded into the sequence of discharge timing. The neuron fires in response to specific segments in the input signal such as those that are ''supratransition.'' Thus, rather than simply

transmitting the input it receives, the neuron is performing a feature extraction. For instance, for neurons receiving converging stimuli from a large number of other neurons, these supratransition excursions may be due to almost synchronous firing of upstream units, and detecting such coincidences has been proposed as one means of signal processing in some areas of the nervous systems [35]. In this setting, the functional role played by the noise could be to increase neuronal sensitivity to such coincidences.

V. CONCLUSION

We reported an effect of noise that is different compared with linearization, as we showed that noise can also improve neuronal reliability. This phenomenon can be potentially beneficial for temporal coding, which relies on precise discharge times. For example, on the one hand, at the level of a single neuron, repeated presentation of the same stimulus signal would elicit reliably the same spike sequence. On the other hand, at the level of an ensemble of neurons receiving the same stimulus, noise can enhance the synchrony of the discharges among the constituting units. Furthermore, our analysis also clarified the mechanism underlying noise-enhanced reliability, by relating it to a noise-induced transition that takes place in neuronal models when the noise intensity is increased, and which separates the regimes in which noise increases the sensitivity of neurons from those in which noise-induced firing dominates. This characterization, together with the description of the dependence of the optimal noise level on input frequency, should prove helpful in determining whether nervous systems operate in regimes where noise-enhanced reliability can possibly take place.

APPENDIX: THE HH EQUATIONS

In an ensemble of HH equations comprising N units, the dynamics of the ith unit are determined by the following system of differential equations [17]:

$$C_m \frac{dV_i}{dt} = g_{\mathrm{Na}} m_i^3 h_i (V_{\mathrm{Na}} - V_i) + g_{\mathrm{K}} n_i^4 (V_{\mathrm{K}} - V_i) + g_{\mathrm{L}} (V_{\mathrm{L}} - V_i) + A s(t) + \xi_i(t),$$

$$\frac{dm_i}{dt} = \alpha_m(V_i) - \gamma_m(V_i) m_i,$$

$$\frac{dh_i}{dt} = \alpha_h(V_i) - \gamma_h(V_i) h_i,$$

$$\frac{dn_i}{dt} = \alpha_n(V_i) - \gamma_n(V_i) n_i, \tag{A1}$$

where the variables V_i, m_i, h_i, and n_i are the membrane potential, the activation, and inactivation of the sodium current, and the activation of the potassium current. V_{Na}, V_{K}, and V_{L} are the reversal potentials of the sodium, potassium, and leak currents, and g_{Na}, g_{K}, and g_{L} are the corresponding maximal conductances. $s(t)$ is the input current. For periodic stimulus $s(t) = \sin(\Omega t)$ and for aperiodic stimulus $s(t)$ is a sample path of a centered Ornstein-Uhlenbeck process with time constant $\tau = 1$ ms and standard deviation $1/\sqrt{2}$. A denotes the amplitude of the stimulus. $\xi_i(t)$ represents white Gaussian noise satisfying $E[\xi_i(t)] = 0$ and $E[\xi_i(t)\xi_j(s)] = \sigma^2 \delta(t-s)$.

The auxiliary functions α_m, α_h, α_n, γ_m, γ_h, and γ_n are:

$$\alpha_m(V) = \Phi \left\{ \frac{0.1(25-V)}{\exp\left[\frac{25-V}{10}\right] - 1} \right\},$$

$$\gamma_m(V) = \Phi \left\{ \alpha_m(V) + 4 \exp\left[-\frac{V}{18} \right] \right\},$$

$$\alpha_h(V) = \Phi \left\{ 0.07 \exp\left[-\frac{V}{20} \right] \right\},$$

$$\gamma_h(V) = \Phi \left\{ \alpha_h(V) + \frac{1}{\exp\left[\frac{30-V}{10}\right] + 1} \right\},$$

$$\alpha_n(V) = \Phi \left\{ \frac{0.01(10-V)}{\exp\left[\frac{10-V}{10}\right] + 1} \right\},$$

$$\gamma_n(V) = \Phi \left\{ \alpha_n(V) + 0.125 \exp\left[-\frac{V}{80} \right] \right\},$$

where Φ is a factor for temperature $\exp[(T/10 - 0.63)\ln 3]$.

Parameter values used in this text are $C_m = 1.0\ \mu\mathrm{F/cm}^2$, $g_{\mathrm{Na}} = 120$ mυ/cm^2, $g_{\mathrm{K}} = 36$ mυ/cm^2, $g_{\mathrm{L}} = 0.3$ mυ/cm^2, $\Phi = 1$, $V_{\mathrm{Na}} = 115$ mV, $V_{\mathrm{K}} = -12$ mV, and $V_{\mathrm{L}} = 10.613$ mV. The parameter values were set so that the resting potential is at $V = 0$ mV.

[1] A.V. Holden, *Lecture Notes in Biomathematics 12* (Springer-Verlag, Berlin, 1976).

[2] J.P. Segundo, J.-F. Vibert, K. Pakdaman, M. Stiber, and O. Diez-Martínez, in *Origins: Brain and Self Organization*, edited by K. Pribram (Lawrence Erlbaum Associates, Hillsdale, NJ, 1994).

[3] J.K. Douglass, L. Wilkens, E. Pantazelou, and F. Moss, Nature (London) **365**, 337 (1993); J.E. Levin and J.P. Miller, *ibid.* **380**, 165 (1996); X. Pei, L. Wilkens, and F. Moss, J. Neurophysiol. **76**, 3002 (1996); J.J. Collins, T.T. Imhoff, and P. Grigg, *ibid.* **76**, 642 (1996).

[4] C. Ivey, A.V. Apkarian, and D.R. Chialvo, J. Neurophysiol. **79**, 1879 (1998).

[5] D.F. Russell, L.A. Wilkens, and F. Moss, Nature (London)

402, 291 (1999).
[6] R.P. Morse and E.F. Evans, Nat. Med. **2**, 928 (1996); P. Cordo, J.T. Inglis, S. Verschueren, J.J. Collins, D.M. Merfeld, S. Rosenblum, S. Buckley, and F. Moss, Nature (London) **383**, 769 (1996); J.J. Collins, T.T. Imhoff, and P. Grigg, *ibid.* **383**, 770 (1996).
[7] J.J. Collins, C.C. Chow, and T.T. Imhoff, Nature (London) **376**, 236 (1995).
[8] D.R. Chialvo, A. Longtin, and J. Müller-Gerking, Phys. Rev. E **55**, 1798 (1997).
[9] T. Shimokawa, A. Rogel, K. Pakdaman, and S. Sato, Phys. Rev. E **59**, 3461 (1999).
[10] C.E. Carr, Annu. Rev. Neurosci. **16**, 223 (1993).
[11] H. Bryant and J.P. Segundo, J. Physiol. (London) **260**, 279 (1976); J. Kröller, O.J. Grüsser, and L.R. Weiss, Biol. Cybern. **60**, 131 (1988); G.A. Cecchi, M. Sigman, J.M. Alonso, L. Martinez, D.R. Chialvo, and M.O. Magnasco, Proc. Natl. Acad. Sci. U.S.A. **97**, 5557 (2000); J. Haag and A. Borst, J. Neurosci. **17**, 4809 (1998); M.J. Berry and M. Meister, *ibid.* **18**, 2200 (1998); P. Reinagel and R.C. Reid, *ibid.* **20**, 5392 (2000).
[12] Z.F. Mainen and T.J. Sejnowski, Science **268**, 1503 (1995).
[13] J.D. Hunter, J.G. Milton, P.J. Thomas, and J.D. Cowan, J. Neurophysiol. **80**, 1427 (1998).
[14] K. Pakdaman, S. Tanabe, and T. Shimokawa, Neural Networks (to be published).
[15] M.N. Shadlen and W.T. Newsome, Curr. Opin. Neurobiol. **4**, 569 (1994); M.N. Shadlen and W.T. Newsome, J. Neurosci. **18**, 3870 (1998).
[16] J.A. White, J.T. Rubinstein, and A.R. Kay, Trends Neurosci. **23**, 131 (2000).
[17] A.L. Hodgkin and A.F. Huxley, J. Physiol. **117**, 500 (1952).
[18] X. Pei, L. Wilkens, and F. Moss, Phys. Rev. Lett. **77**, 4679 (1996).
[19] S. Tanabe, S. Sato, and K. Pakdaman, Phys. Rev. E **60**, 7235 (1999).
[20] S. Tanabe and K. Pakdaman, Biol. Cybern (to be published).
[21] W.E. Sullivan and M. Konishi, J. Neurosci. **4**, 1787 (1984); **393**, 268 (1998).
[22] G. Rose and W. Heiligenberg, Nature (London) **318**, 178 (1985).
[23] D. Ferster and B. Jagadeesh, J. Neurosci. **12**, 1262 (1992); L.G. Nowak, J.V. Sanchez-Vives, and D.A. McCormick, Cereb. Cortex **7**, 487 (1997).
[24] S. Tanabe, T. Shimokawa, S. Sato, and K. Pakdaman, Phys. Rev. E **60**, 2182 (1999).
[25] C. Kurrer and K. Schulten, Phys. Rev. E **51**, 6213 (1995);
[26] K. Wiesenfeld, D. Pierson, E. Pantazelou, C. Dames, and F. Moss, Phys. Rev. Lett. **72**, 2125 (1994); S. Shinomoto and Y. Kuramoto, Prog. Theor. Phys. **75**, 1105 (1986).
[27] R.L. Stratanovich, in *Topics in the Theory of Random Noise, Volume II* (Gordon and Breach, Science Publisher, New York, 1967).
[28] An approximate solution of the FPE was obtained by solving numerically the system of ordinary differential equations for the truncated Fourier coefficients of $n(\varphi,t)$ [19,20]. Numerical simulations were carried out using the Runge-Kutta scheme. Controls were run with the Euler scheme, with an adequate time step. The flux computed with the two methods agreed.
[29] S. Tanabe, and K. Pakdaman, Phys. Rev. E **63**, 031911 (2001).
[30] M. I. Freidlin and A. D. Wentzell, *Random Perturbations of Dynamical Systems*, 2nd ed. (Springer, Berlin, 1998).
[31] An approximate solution of the expansion of the FPE was obtained by solving numerically the system of ordinary differential equations for the truncated Fourier coefficients of the $n_k(\varphi,t)$. For the sake of clarity of the numerical algorithm, the forward Euler scheme was used. The expansion of the flux computed with this scheme was in agreement with the flux computed directly from the FPE using the Runge-Kutta algorithm [28].
[32] T. Shimokawa, K. Pakdaman, and S. Sato, Phys. Rev. E **59**, 3427 (1999).
[33] D.H. Perkel and T.H. Bullock, Neurosci. Res. Program Bull. **6**, 221 (1968).
[34] F. Rieke, D. Warland, Rob de Ruyter van Steveninck, and W. Bialek, *Spikes, Exploring the Neural Code* (MIT Press, Cambridge, MA, 1997).
[35] P. König, A.K. Engel, and W. Singer, Trends Neurosci. **19**, 130 (1996).